JOURNAL OF COLLOID AND INTERFACE SCIENCE 193, 17–25 (1997)
ARTICLE NO. CS975046

The Effect of Overlap between Monomers on the Determination of Fractal Cluster Morphology

C. Oh and C. M. Sorensen[1]

Department of Physics, Kansas State University, Manhattan, Kansas 66506-2601

Received December 16, 1996; accepted June 20, 1997

Diffusion limited cluster aggregate (DLCA) morphology is studied as a function of monomeric particle overlap for finite sized clusters. The morphology is parameterized by both the fractal dimension D and the prefactor k_0. For clusters created on a three-dimensional cubic lattice we find $D = 1.80 \pm 0.03$ and $k_0 = 1.30 \pm 0.07$ when the spherical monomers are in point contact. Both these values increase as overlap increases. Also presented is an analysis of the two-dimensional projection of these clusters in order to facilitate electron micrograph images of real clusters. Quantitative relations between actual three-dimensional cluster parameters such as cluster radius of gyration, fractal dimension and number of monomers per aggregate, and measurable two-dimensional quantities such as longest lengths and projected area are given as a function of monomer overlap. Relationships between lengths can be explained only by use of the proper density correlation function and accounting for cluster anisotropy. Finally, we make an unsuccessful attempt to find the source of recent experimental discrepancies in the prefactor k_0 in terms of a possible unknown degree of overlap. © 1997 Academic Press

I. INTRODUCTION

It is well established that random aggregation of fine particles leads to clusters with fractal morphology if particle coalescence does not occur (1–6). Most commonly, colloidal or aerocolloidal systems aggregate via the process of diffusion limited cluster aggregation (DLCA) which yields clusters with a fractal dimension of $D \simeq 1.78$. It is convenient to describe this structure with the equation

$$N = k_0\left(\frac{R_g}{a}\right)^D, \qquad [1]$$

where N is the number of monomers in a cluster, R_g is the cluster radius of gyration, a is the monomer radius, and k_0 is a prefactor of order unity (7). The structure is parameterized by both the fractal dimension D and the prefactor k_0. A considerable body of previous work has found $D \simeq 1.78$ for a variety of colloidal and aerocolloidal aggregates including soot. Until recently, however, the prefactor has been ignored. Its accepted importance has been increasing because of its relation to cluster mass, transport, and light scattering properties. Wu and Friedlander (8) reviewed a variety of simulation and real system data to find that k_0 was of order unity. Work from this laboratory has measured $k_0 = 1.23 \pm 0.07$ (9) and 1.66 ± 0.4 (6) for soot from two different flames and our DLCA simulations have found $k_0 = 1.2 \pm 0.15$ (10). In contrast, Samson *et al.* (4) found $D \simeq 1.44$ and $k_0 \simeq 3.4$ using stereo views of 3d aggregates. Using the data of Samson *et al.*, Puri *et al.* (11) also found $D \simeq 1.40$ and $k_0 \simeq 3.5$. Independently, Koylu *et al.* (12) found $D \simeq 1.64$ and $k_0 \simeq 2.4$ using stereo views of 3d aggregates and have supported this value of k_0 with subsequent studies (13–15). Considering the role of D and k_0 in describing light scattering from fractal aggregates it is important to rectify the discrepancies among the experimental values.

With this motivation and given the simulation result of $k_0 = 1.2$ we ask, how could the morphology of soot differ from flame to flame and especially from ideal aggregates as some of the results above imply? Perhaps the answer to this question lies in the "necking" or overlap between monomers often observed in soot clusters. By "necking" we mean nonpoint contacts between adjoining monomers which are approximately spherical. In this paper we described simulated clusters with a variable amount of monomer overlap and compute the effects of this overlap on k_0 and D. This study is not only relevant to the morphological description of soot through Eq. [1], but it is also valuable for the morphological description of aggregates of many materials at various stages of sintering (16, 17). This is so because a simple description of the extent of sintering is the degree to which adjacent monomers merge. Thus the first task of this paper is to find how k_0 and D depend on monomer overlap.

Very often the morphology of clusters must be determined from their projected two-dimensional images. Thus there has been previous work, both analytic and simulation, which has attempted to determine how the true, three-dimensional parameters N, R_g, and D are related to measurable two-dimensional parameters such as the projected cluster area, projected radius of gyration, and projected longest length

[1] To whom correspondence should be addressed.

0021-9797/97 $25.00

(4, 6, 7, 12, 18–20). We do this again here with this background as a guide and establish how to proceed from projected to true values. We also do this for clusters with variable monomer overlap since this is relevant to the prefactor discrepancy described above and for future work on sintered aggregates.

In summary, the work here has value in three areas:

1. We describe how k_0 and D depend on the degree of monomer overlap in a cluster.
2. We establish how to use two-dimensional projected cluster data to determine true three-dimensional cluster parameters for clusters with monomers of arbitrary overlap (including point contacts).
3. We apply these first two abilities to attempt to understand the prefactor discrepancies.

II. COMPUTER SIMULATION

The DLCA simulation was performed on a $L \times L \times L$ cubic lattice with periodic boundary conditions (3, 21). Initially, n_0 monomers were randomly placed (avoiding multiple occupancy and nearest neighbor contact) on L^3 lattice sites, which yields the monomer density $\rho = n_0/L^3$. Therefore at the beginning of the simulation there were n_0 "clusters" each with a single monomer. Then at each step of the simulation, one cluster was randomly selected with equal probability and moved by one lattice step in one of the six possible directions ($\pm x$, $\pm y$, $\pm z$) chosen randomly. While moving, if two or more clusters came into contact with each other, they were joined permanently to form a larger cluster. A contact was considered to be made if a monomer of one cluster occupied a lattice site adjacent to a monomer of another cluster. The process was repeated for a prescribed number of steps. The simulation was performed twice with $\rho = 0.001$ and once with $\rho = 0.002$. In our simulations we used $L = 100$. The product of the three simulations was 186 clusters of size ranging from $N = 2$ to 580. Monomers still left at the end of the simulations were discarded because they have no bearing on the current problem.

III. DATA ANALYSIS AND RESULTS

When two monomers overlap it means that the distance between them is not equal to the sum of the two radii. To quantify the overlap between monomers an overlap parameter δ is defined as

$$\delta = \frac{2a}{\ell}, \qquad [2]$$

where a is the monomer radius and ℓ is the lattice spacing as shown in Fig. 1. Here we assume a monodisperse monomer size distribution. If $\delta = 1$, the monomers are in point contact. If δ is larger than 1, there is overlap between monomers. If δ is less than 1, then the monomers are not in contact with each other, something like dew drops hanging on a spider web. Even though this latter situation may not, as yet, have any practical importance, it still poses an interesting theoretical question.

To study the effect of the overlap, we need to obtain the three-dimensional information of a cluster. This was done by putting a spherical monomer of radius a at each monomer position of a cluster. The cluster was then digitized with a finer lattice (Γ space) with the lattice spacing $\gamma = \ell/8$.

III.1. δ and R_g

The radius of gyration R_g was calculated in Γ space as

$$R_g^2 = \frac{1}{n} \sum_i (\mathbf{r}_i - \mathbf{r}_{cm})^2. \qquad [3]$$

Here $\mathbf{r}_{cm}$ is the position of the center of mass of a cluster, $\mathbf{r}_i$ is a position of a lattice point within the cluster, and n is the number of lattice points within the cluster in Γ space; i.e., n is the volume of a cluster. R_g calculated in Γ space was appropriately normalized with the monomer radius a. As a result, we obtained R_g/a dependent only on $\delta = 2a/\ell$, but not on γ.

Since we have the true N and, from Eq. [3], the true R_g, we can determine D and k_0 through Eq. [1]. Figure 2 shows $\log(R_g/a)$ vs $\log N$ for $\delta = 1$ and 2. Note the linearity of the $\delta = 2$ plot. On a log–log plot this linearity implies that Eq. [1] still provides an accurate description of the cluster despite the large overlap. Hence from this perspective the cluster is still a fractal. By fitting the data to Eq. [1] for $N = 5$ to 580, we obtain D and k_0 as a function of δ. The results are summarized in Fig. 3. For $\delta = 1$ we have $D =$

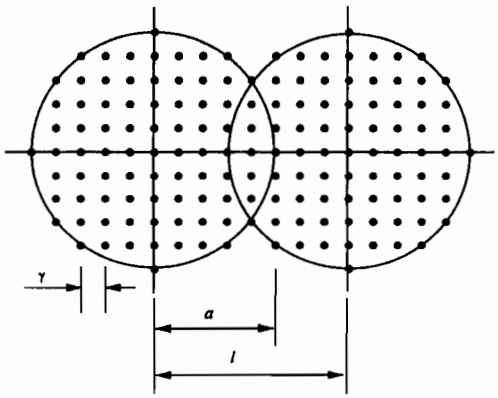

FIG. 1. A pair of overlapping monomers digitized with a resolution $\gamma = \ell/8$. Dots represent the occupied sites in Γ space. a is the monomer radius and ℓ is the lattice spacing in real space (in which the DLCA simulation was performed).

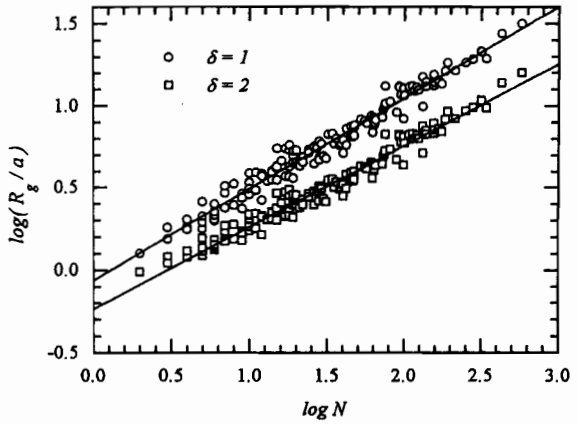

FIG. 2. Cluster radius of gyration normalized by the monomer radius versus number of monomers per cluster for two different overlap parameters, $\delta = 1$ (point contacts) and $\delta = 2$.

1.80 ± 0.03 and $k_0 = 1.30 \pm 0.07$. These values are in excellent agreement with the known values of D from a large body of previous work and with the value of $k_0 = 1.26 \pm 0.15$ from previous on-lattice simulations from our laboratory (10). For our largest overlap, $\delta = 2$, we find, for these finite sized clusters, $D = 2.01 \pm 0.03$ and $k_0 = 3.0 \pm 0.08$; thus, overlap thickens or densifies the clusters. By extrapolating the curves in Fig. 3 to $\delta = 0$, we find $D \approx 1.75$ and $k_0 \approx 0$.

The behavior of D and k_0 as a function of δ in Fig. 3 can be explained as follows. Let $k_0(\delta)$, $R_g(\delta)$, and $D(\delta)$ be the prefactor, the radius of gyration, and the fractal dimension of a cluster, respectively, for an arbitrary overlap δ. Then for $\delta = 1$ we have

$$N = k_0(1)\left(\frac{R_g(1)}{\ell/2}\right)^{D(1)}. \qquad [4]$$

By comparing Eq. [4] with Eq. [1], we get the prefactor for an arbitrary δ:

$$k_0(\delta) = k_0(1)\,\frac{a^{D(\delta)}}{(\ell/2)^{D(\delta)}}\,\frac{(R_g(1)/\ell/2)^{D(1)}}{(R_g(\delta)/\ell/2)^{D(\delta)}}. \qquad [5]$$

Now let $R_{g,lattice}$ be the radius of gyration of a cluster made of point monomers. If the monomers are finite sized but do not overlap, the cluster radius of gyration is given by $R_g^2 = R_{g,lattice}^2 + R_{g,monomer}^2$. If the monomers are spherical, $R_{g,monomer}^2 = 3a^2/5$. Then for an arbitrary δ, $R_g(\delta)$ can be approximated as

$$R_g(\delta) \simeq \left[R_{g,lattice}^2 + \frac{3}{5}a^2\right]^{1/2}. \qquad [6]$$

For $\delta \leq 1$ Eq. [6] is exact; for $2 > \delta > 1$ it is a good approximation. If $a \ll R_{g,lattice}$, and using Eq. [2], we have

$$R_g(\delta) \simeq R_{g,lattice}\left[1 + \frac{3}{10}\delta^2\left(\frac{\ell/2}{R_{g,lattice}}\right)^2\right]. \qquad [7]$$

Since $\ell/2R_{g,lattice} \to 0$ for $N \to \infty$, $R_g(\delta)$ becomes independent of δ and

$$R_g(\delta) \simeq R_{g,lattice} \qquad [8]$$

for large N. Furthermore, due to self-similarity as $N \to \infty$, $D(\delta)$ becomes independent of δ; i.e., $D(\delta) \simeq D$. So in the limit $N \to \infty$ Eq. [5] yields the asymptotic form of k_0,

$$k_{0,\infty}(\delta) = k_0(1)\delta^D, \qquad [9]$$

where $k_{0,\infty}(\delta)$ is the value of k_0 for $N \to \infty$ for an arbitrary δ. The dotted line in Fig. 3 shows $k_{0,\infty}(\delta)$ with $k_0(1) = 1.30$ and $D = 1.80$ and a reasonable agreement is seen for $\delta \leq 1$.

According to Eq. [7], if $\delta < 1$, $R_g(\delta)/R_{g,lattice}$ does not change much since this ratio is unity plus a factor proportional to δ^2. This insensitivity of $R_g(\delta)$ on δ is responsible for the apparent insensitivity of $D(\delta)$ on δ shown in Fig. 3 for $\delta \leq 1$. Since the monomers do not touch each other for $\delta < 1$, it may be natural that $D(\delta)$ does not depend strongly on δ. The constancy of $D(\delta)$ aids the good agreement between $k_{0,\infty}(\delta)$ of Eq. [9] and k_0 from simulation for $\delta \leq 1$. For $\delta > 1$ monomers start to overlap, and the clusters become more compact. As a result, the apparent $D(\delta)$ increases rapidly with δ. According to Eq. [7] for a finite size cluster $R_g(\delta)/R_{g,lattice}$ increases above unity with an additive factor proportional to δ^2. According to Eq. [5] increasing $D(\delta)$ and $R_g(\delta)$ means that k_0 should become smaller and hence a deviation from $k_{0,\infty}(\delta)$ as seen.

Finally we remark that for asymptotically large clusters, $N \to \infty$, D should be independent of overlap as long as the monomer radius is much less than the cluster radius. Thus

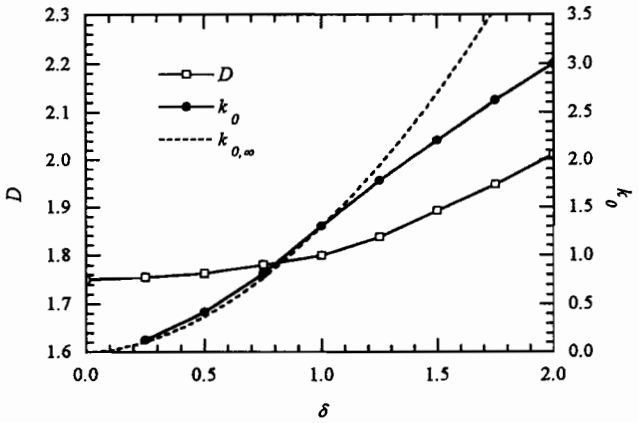

FIG. 3. Fractal dimension D and prefactor k_0 for DLCA clusters as a function of overlap parameter δ. Dashed line is calculated k_0 by Eq. [9].

in this limit only k_0 is sensitive to overlap. Note that the anticorrelation between D and k_0 implied by Eq. [1] also accounts for the discrepancy between the simulated k_0 and the predicted $k_{0,\infty}(\delta)$ since if $D = 1.8$ for $\delta > 1$, smaller than the simulated values plotted in Fig. 3, then k_0 would be larger hence closer to the predicted value.

III.2. The Number of Monomers and the Projected Area

For a self-similar fractal cluster the number of monomers should scale with any characteristic length with the same fractal dimension. So if R_2 is half of the largest length of the projected image and a is the monomer radius, then in analogy to Eq. [1] we expect

$$N = k_2\left(\frac{R_2}{a}\right)^D, \qquad [10]$$

where D is the fractal dimension and k_2 is a prefactor of order 1. If the fractal dimension of the projected image is D_p, then we expect the cluster projected area A_c to be related to R_2 as

$$\frac{A_c}{A_a} = \beta\left(\frac{R_2}{a}\right)^{D_p}, \qquad [11]$$

where β is another prefactor of order 1, and A_a is the projected area of the monomer. By combining Eqs. [10] and [11], we find the relation between the number of monomers and the projected area to be

$$N = k_a\left(\frac{A_c}{A_a}\right)^{\alpha}, \qquad [12]$$

where $k_a = k_2/\beta^{D/D_p}$ is a constant of order unity and $\alpha = D/D_p$ is the ratio between the fractal dimensions of the cluster and its projected image. We have found this result previously by another argument and have shown its reasonableness (6). It has been argued that for $D < 2$, $D_p = D$ but this can only strictly apply when $N \to \infty$. For typical soot clusters ($N \sim 100$) one finds D_p to be about 10% smaller than D (4, 6). Consequently, the value of α is about 1.1. Indeed, this is the value found empirically for Eq. [12] dating back to the original work by Medalia and Heckman (18). Equation [12] has played a major role in the TEM analysis of aggregates. It also provides an important clue to the understanding of the diffusive transport of fractal aggregates (22, 23).

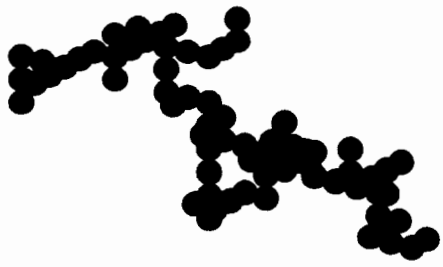

FIG. 4. Random projection of a three-dimensional DLCA aggregate onto a plane with overlap parameter $\delta = 1$; i.e., the monomers do not overlap but have point contacts. Note, however, the apparent overlap due to the projection.

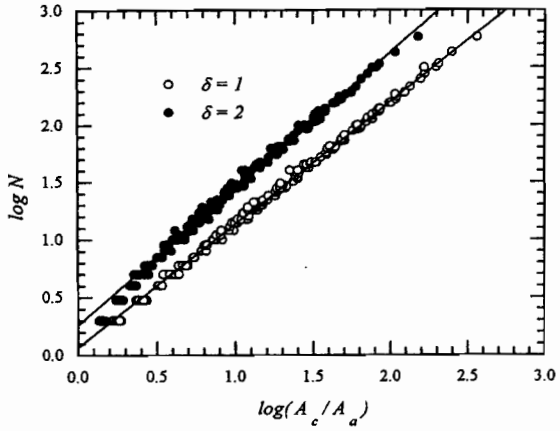

FIG. 5. The ratio of the cluster projected area to the monomer projected area as a function of the number of monomers per cluster for two different overlap parameters $\delta = 1$ (point contacts) and $\delta = 2$.

We tested Eq. [12] with our simulated clusters with the overlap between monomers as a variable. To calculate A_c the clusters were rotated by random angles around three orthogonal axes. Then the clusters were projected onto three orthogonal planes and the projected areas were averaged. Figure 4 shows a projected image of a cluster for $\delta = 1$, i.e., monomers in point contact. Even for $\delta = 1$ the projected image looks as if there is some degree of overlap between monomers. This fact clearly demonstrates the difficulty of determining δ from a TEM picture.

Figure 5 illustrates the relation between A_c/A_a and N for $\delta = 1$ and 2 obtained with our simulated clusters. By fitting the data to Eq. [12] for $N = 5$ to 580, we find $k_a = 1.17 \pm 0.02$ and $\alpha = 1.07 \pm 0.005$ for $\delta = 1$. These values show reasonable agreement with the result of Köylü *et al.* (12), who found $k_a = 1.15 \pm 0.18$ and $\alpha = 1.09 \pm 0.02$ from a TEM analysis of soot particles. For $\delta = 2$ we find $k_a = 1.81 \pm 0.03$ and $\alpha = 1.19 \pm 0.01$.

This increase in k_a and α with δ can be explained as follows. As δ increases from δ_1 to δ_2, A_a increases as

$$A_{a,2} = \left(\frac{\delta_2}{\delta_1}\right)^2 A_{a,1}. \qquad [13]$$

However, A_c is not going to increase as much because of the overlap between monomers; i.e.,

$$A_{c,2} < \left(\frac{\delta_2}{\delta_1}\right)^2 A_{c,1}. \qquad [14]$$

So as δ increases, the ratio of the projected images A_c/A_a decreases. According to Eq. [12] for constant N if A_c/A_a decreases with increasing δ, α and/or k_a should increase to keep N the same.

Figure 5 shows that the difference in N for a given A_c/A_a could be as much as a factor of 2 when δ changes from 1 to 2. Consequently, the estimation of N from A_c/A_a is sensitive to the value of δ. Moreover, the difference seems to be increasing with N. Although it is not clearly visible in Fig. 5, the slope of A_c/A_a vs N curve changes as N increases. So the estimation of N is also sensitive to the range of N. This point is very well illustrated in Fig. 6 which shows three sets of (α, k_a) plotted as a function of δ. They correspond to different starting points (5, 10, 20) of the curve fit, like the one shown in Fig. 5. In the point particle limit, i.e., $\delta \to 0$, there should not be any screening during projection; thus $N = A_c/A_a$ for $\delta \to 0$. This point is correctly represented in Fig. 6 with $k_a \approx \alpha \approx 1$ at $\delta = 0$. For a fixed δ, k_a becomes bigger as the cluster size gets bigger while α gets smaller and approaches 1. Meakin (21) reported a similar behavior of α. This trend implies that in the limit of $N \to \infty$ the fractal dimension of a projected image is the same as that of the cluster if $D < 2$. This does not mean that the monomer–monomer screening is unimportant for large clusters; rather the fact that $k_a > 1$ means that a finite fraction of monomers are screened during projection.

In summary, in order to estimate N correctly from a TEM picture it is necessary to know δ and the range of N before use of Eq. [12]. If $\delta > 1$ in a real cluster, an analysis assuming $\delta = 1$ would yield N too small.

III.3. δ and R_L

In a TEM analysis of clusters it is often useful to define a longest length of the cluster in either three or the projected two dimensions. Half of this length will be designated as R_L with $L = 2$ or 3 for the two-dimensional projection or the real, three-dimensional cluster, respectively. Then in analogy to Eq. [1] one may write

$$N = k_L\left(\frac{R_L}{a}\right)^{D_L}. \qquad [15]$$

If the cluster is self-similar, then $D_L = D$ for $N \to \infty$. R_2 is commonly used because it is easy to obtain from a TEM analysis.

Figure 7 shows R_2/a and R_3/a vs N for $\delta = 1$. The fractal dimensions obtained by fitting the data to Eq. [15] for $N = 5$–580 are $D_2 = 1.77 \pm 0.03$ and $D_3 = 1.77 \pm 0.03$. These values agree with $D = 1.80 \pm 0.03$ obtained using R_g within the statistical uncertainty and hence are consistent with self-similarity. Figure 8 shows the behavior of D_2 and D_3 as a function of δ. The figure shows that the D_Ls are pretty good approximations of the true D for $\delta \geq 1$. This means that we can use R_2 or R_3

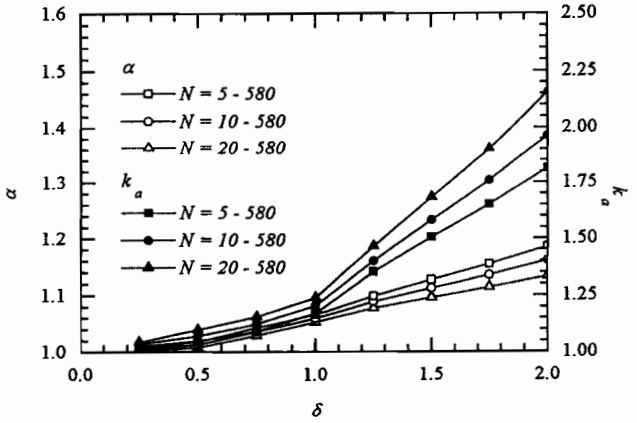

FIG. 6. The parameters α and k_a of Eq. [12] versus overlap parameter for three different fit ranges in N, the number of monomers per cluster.

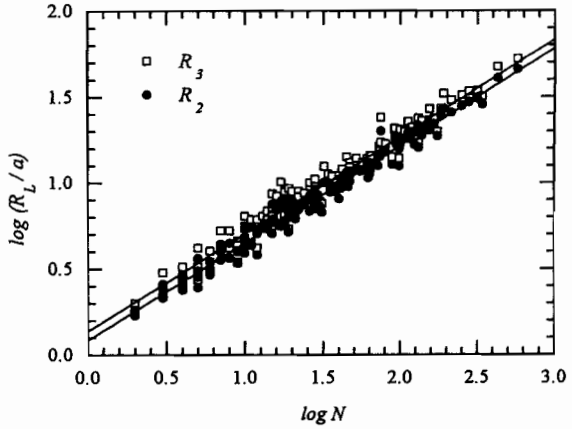

FIG. 7. The ratio of half the cluster longest length in three or two dimensions, R_3 or R_2, respectively, to the monomer radius versus the number of monomers per clusters. The overlap parameter is $\delta = 1$, point contacts.

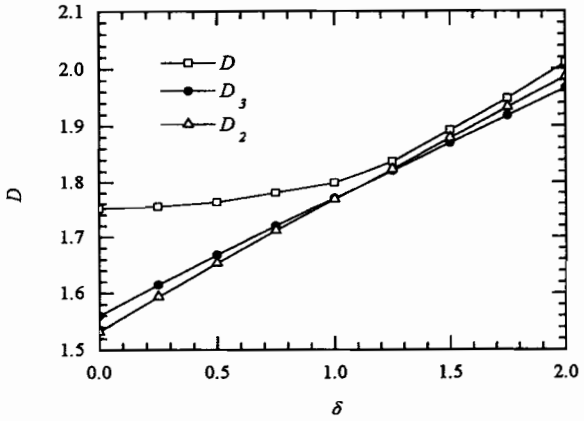

FIG. 8. Fractal dimensions versus overlap parameter. D is determined from the radius of gyration, D_3 from half the longest cluster length in three dimensions, and D_2 from half the longest cluster length when projected into two dimensions.

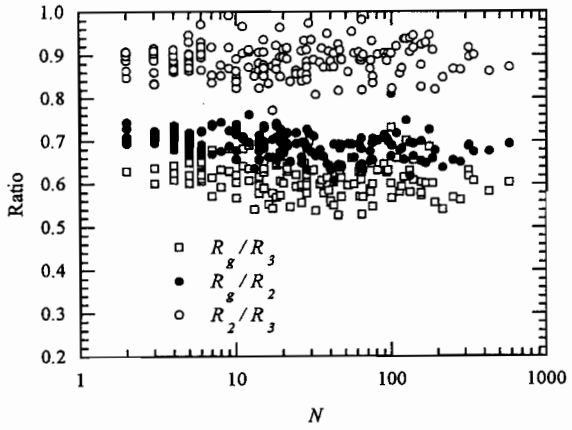

FIG. 9. Various ratios of cluster lengths versus N. The overlap parameter is $\delta = 1$, point contacts.

instead of R_g to obtain the fractal dimension of a cluster. However, for $\delta < 1$ D_Ls become much smaller than D as δ decreases. This behavior can be explained as follows. Let $R_L(a)$ be R_L at a finite a. Then $R_L(a)$ is related to $R_L(0)$ as

$$R_L(a) = R_L(0) + a. \qquad [16]$$

Thus as δ, and consequently a, increases the fractional increase in $R_L(a)$ is bigger for small N clusters. This dependence of $R_L(a)$ on δ makes a log–log plot of N vs R_L increase its slope as δ increases, and the slope is the fractal dimension. Note that this effect is much smaller for R_g because, by Eq. [7], a contributes to the total R_g by a quadratic additive factor rather than the linear additive factor in Eq. [16].

Light scattering measures R_g, whereas TEM pictures yield R_2. The relation between R_g and R_2 is not trivial and as a consequence different authors have different opinions about the relation (15, 22, 24). Here we will consider these relations and test them with our simulation. Figure 9 shows the ratio $\mathcal{R}_L = R_g/R_L$ vs N for $\delta = 1$. The average values are $\langle \mathcal{R}_3 \rangle = 0.61 \pm 0.03$ and $\langle \mathcal{R}_2 \rangle = 0.69 \pm 0.03$ for $N \geq 10$. $\mathcal{R}_L$s were calculated for other δs, too. The results were rather insensitive to δ, except for small $N(N \leq 10)$. Also shown in the figure is the ratio R_2/R_3 for $\delta = 1$. The average of R_2/R_3 was 0.89 ± 0.03. The ratio was also insensitive to δ except for small N.

One approach to understanding these ratios is simply to consider a DLCA cluster as a spherically isotropic cluster of radius R_3 and the density $\rho(r) \sim r^{D-3}$ (15, 19). Then through a simple integration one can show that

$$R_g^2 = \frac{D}{D+2} R_3^2. \qquad [17]$$

For $D = 1.8$ Eq. [1] yields $R_g/R_3 = 0.688$.

This value is about 10% larger than the result of our simulation. If we assume that the projected image is defined with the similar density function for $d = 2$ dimensional space, i.e., $\rho \sim R^{D-2}$, and with $R_2 = R_3$ because of the spherical symmetry, then we find

$$R_{g,2}^2 = \frac{D}{D+2} R_2^2, \qquad [18]$$

where $R_{g,2}$ is the radius of gyration of the projected image. This is the same as Eq. [17]. Equation [18] also yields $R_{g,2}/R_2 = 0.688$ for $D = 1.80$ which is in excellent agreement with our simulation. This excellent agreement, however, must be considered fortuitous because the assumptions that lead to Eq. [18] do not hold. First, it is not clear whether the three-dimensional density $\rho \sim r^{D-3}$ will be $\sim r^{D-2}$ when projected. Second, as discussed above, there is good evidence, at least for small clusters, that projection alters the fractal dimension of the cluster to $D_p = D/\alpha$, where α is the exponent in Eq. [12]. Third, $R_{g,2}$ is the radius of gyration of the projected clusters, undoubtedly different than the true, three-dimensional radius of gyration. Fourth, a DLCA cluster is not spherically isotropic (24). Although it may look isotropic when rotationally averaged, the largest length of the projected image, R_2, is smaller than the largest length of the cluster in three-dimensional space, R_3. Therefore, the use of $R_2 = R_3$ is wrong. Below we present a proper derivation of the relationship between R_g, R_3, and R_2.

A self-similar fractal should be defined with a power law density correlation function $g(r)$, instead of a power law density $\rho(r)$, expressed as

$$g(r) = r^{D-3} h\left(\frac{r}{\xi}\right), \qquad [19]$$

where $h(r/\xi)$ is a cut-off function and ξ is a characteristic length of the cluster. Once $g(r)$ is known, R_g^2 can be calculated from the small q expansion of the total scattered intensity $I(q)$ (25):

$$I(q) = \int e^{i\mathbf{q}\cdot\mathbf{r}} g(r) d^3r. \qquad [20]$$

Using a sphere-like cut-off function (23) one can show that

$$R_g^2 = \frac{2D(D+1)}{(D+2)(D+5)} R_3^2. \qquad [21]$$

For $D = 1.8$ Eq. [21] yields $R_g/R_3 = 0.625$. This value agrees well with our simulation result. Therefore, we prefer Eq. [21] over Eq. [17] to define the relation between R_g and R_3 of a DLCA cluster embedded in three-dimensions.

From a TEM picture one obtains R_2 instead of R_3. To find the relation between R_3 and R_2 we need to know the shape of a cluster. Botet and Jullien (25) described the anisotropic

nature of simulated DLCA clusters using the radius of gyration tensor

$$R_{ij}^2 = \frac{1}{2N} \sum_{\alpha,\beta} r_{\alpha i} r_{\beta j}, \qquad [22]$$

where $(i, j) = 1, 2, 3$ and $(\alpha, \beta) = 1, \ldots, N$.

By diagonalizing the tensor, they showed that a DLCA cluster has three different principal radii of gyration. This implies that DLCA clusters are better represented by an ellipsoid (rather than by a sphere) defined by

$$\frac{x^2}{a^2} + \frac{y^2}{b^2} + \frac{z^2}{c^2} = R_3^2, \qquad [23]$$

where

$$a = \frac{R_x}{R_z} = 0.3162$$

$$b = \frac{R_y}{R_z} = 0.5$$

$$c = 1 \qquad [24]$$

and R_3 is half of the largest length of the cluster in three dimensions. Here we used Botet and Jullien's definition of R_x, R_y, and R_z to obtain a, b, and c.

Now consider the relation between R_2 and R_3. When an ellipsoid is projected onto a plane, the longest axis is most important in determining the length of the projected image, the second longest axis is next important, and the shortest axis is least important. Therefore, for the simplicity of the calculation let us assume that the second longest and the shortest axes are the same; i.e.,

$$a = b = 0.5. \qquad [25]$$

Suppose the ellipsoid is projected along an arbitrary direction $\hat{z}$ onto xy plane perpendicular to $\hat{z}$. Now put the y axis on the plane defined by $\hat{z}$ and the direction of the long axis of the ellipsoid as shown in Fig. 10. Then the projected image will have its maximum length along the y axis. After a simple calculation, we find

$$\frac{R_2}{R_3} = [b^2\cos^2\theta + c^2\sin^2\theta]^{1/2}, \qquad [26]$$

where θ is the angle between $\hat{z}$ and the long axis as shown in Fig. 10. After averaging over the orientation, we obtain

$$\left\langle \frac{R_2}{R_3} \right\rangle = \frac{1}{2}(c^2 - b^2)^{1/2}\left[(\alpha^2 - 1)^{1/2} + \frac{\alpha^2}{2}\sin^{-1}\frac{1}{\alpha}\right], \qquad [27]$$

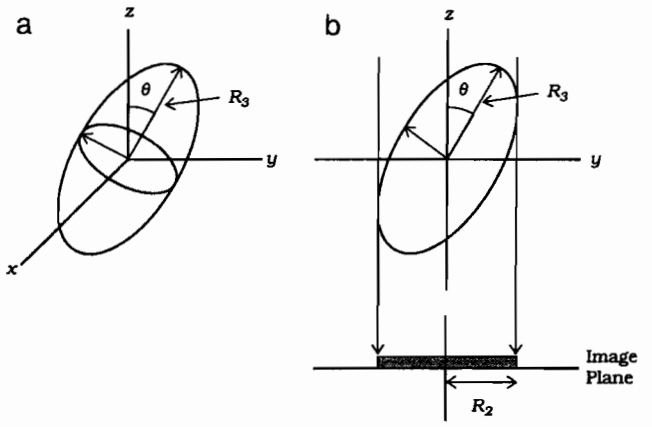

FIG. 10. Diagram of ellipsoids and their two-dimensional projection. (a) Three-dimensional ellipsoid with its semimajor axis R_3 in the yz plane. (b) The ellipsoid along the x axis. Micrograph imaging is represented by a projection along the z axis onto TEM image plane which is parallel to the xy plane. R_2 is half the longest length of the projected image.

where $\alpha^2 = c^2/(c^2 - b^2)$. For $b = 0.5$ and $c = 1$ we obtain

$$\left\langle \frac{R_2}{R_3} \right\rangle = 0.87. \qquad [28]$$

This value agrees well with the result of our simulation shown in Fig. 9. By putting Eqs. [21] and [28] together we obtain the relation between R_g and R_2,

$$\left\langle \frac{R_g}{R_2} \right\rangle = \left[\frac{2D(D+1)}{(D+2)(D+5)}\right]^{1/2}\left\langle \frac{R_3}{R_2} \right\rangle$$

$$= 0.718, \qquad [29]$$

for $D = 1.80$. This value shows good agreement with the ratio $\langle \mathcal{R}_2 \rangle$ obtained in our simulation. We believe this agreement is another evidence that DLCA clusters should be considered as an ellipsoid.

Given that the relations between R_g and the R_Ls are established, the relations between k_0 and k_Ls can be determined. Assuming that R_g and R_L scale with the same D and using Eqs. [1] and [15] we have

$$k_L(\delta) = k_0(\delta)\langle \mathcal{R}_L \rangle^D. \qquad [30]$$

The various prefactors obtained in our analysis of the simulated clusters are plotted in Fig. 11. For $\delta = 1$, we find $k_2 = 0.7$ and $k_3 = 0.6$, values significantly less than unity (15, 22).

III.4. $R_{g,exp}$ and N_{exp}

In a TEM analysis Eqs. [12] and [29] may be used to obtain the number of monomers in a cluster and the radius of gyration of the cluster. Here we determine what error in

D and k_0 would be incurred if, in fact, $\delta \neq 1$ yet the analysis proceeded under the $\delta = 1$ assumption. For $\delta = 1$ Eq. [12] becomes

$$N_{\text{exp}} = 1.15\left(\frac{A_c}{A_a}\right)^{1.07}, \qquad [31]$$

where N_{exp} is the experimental value of N, and Eq. [36] with the simulation numerical value yields the experimental value of R_g,

$$R_{g,\text{exp}} = 0.69R_2. \qquad [32]$$

By combining Eqs. [31] and [32] we obtain

$$N_{\text{exp}} = k_{\text{exp}}\left(\frac{R_{g,\text{exp}}}{a}\right)^{D_{\text{exp}}}, \qquad [33]$$

where k_{exp} and D_{exp} are the experimental values of k_0 and D, respectively.

In order to test the validity of this analysis we applied Eqs. [31]–[33] to our simulated clusters. k_{exp} and D_{exp} obtained from the analysis are plotted in Fig. 12 along with k_0 and D obtained from the true N vs the true R_g plots. For $\delta \leq 1$ the experimental values agree well with the true values. However, for $\delta > 1$ the agreement is not good. Interestingly, k_{exp} and D_{exp} show very little dependence on δ. The implication is that the $\delta = 1$ analysis applied to $\delta > 1$ clusters would not see the effects of the overlap on the cluster morphology as described by k_0 and D. In fact, these values would look much like the values for a $\delta = 1$ cluster. For example, for a large overlap of $\delta = 2$ the true values from a three-dimensional analysis (Fig. 3) are $k_0 = 3.0$ and $D = 2.01$, whereas the projected clusters analyzed under the assumption of $\delta = 1$, Eqs. [31]–[33], yield $k_{\text{exp}} = 1.8$ and $D = 1.78$. So the error incurred is significant. On the other hand, note that these "experimental" values are close to the true values when there is no monomer overlap, $k_0 = 1.30$ and $D = 1.80$; in fact the fractal dimension is essentially the same. This implies that if real clusters have overlap but are analyzed assuming no overlap, their k_0 and D values will be similar to clusters with no overlap. Instead the fractal dimensions obtained in the stereo analysis were smaller than the accepted value. We therefore conclude that monomer overlap does not explain the large experimental values of k_0 relative to simulation.

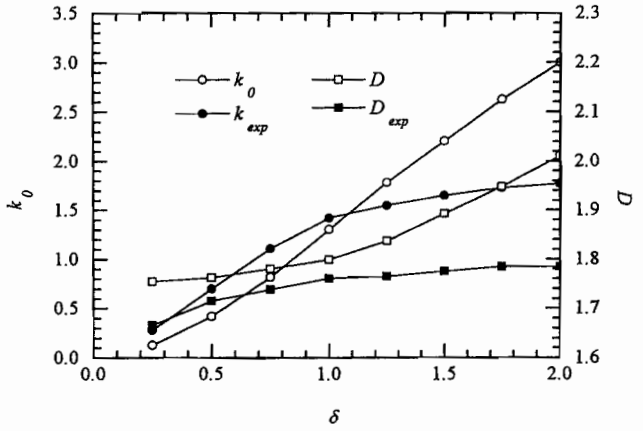

FIG. 12. Actual prefactor and fractal dimension, k_0 and D, respectively, of the three-dimensional cluster, and experimental prefactor and fractal dimension, k_{exp} and D_{exp}, respectively, versus overlap parameter. The experiment values were determined by the analysis of Eqs. [31]–[33] which assume $\delta = 1$.

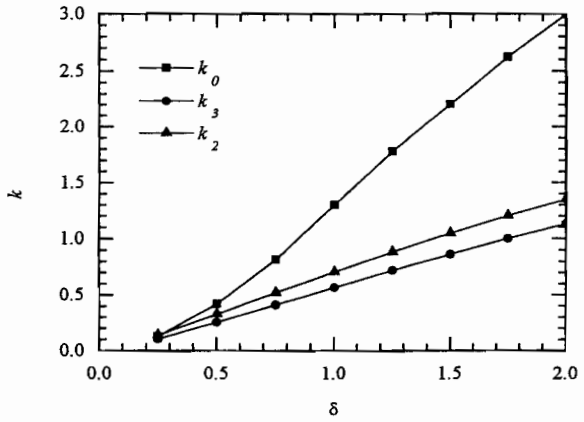

FIG. 11. Various prefactors versus overlap parameter.

IV. CONCLUSIONS

The fractal dimension and prefactor have been studied as a function of monomer overlap for finite sized, DLCA clusters simulated on a three-dimensional cubic lattice. Also, in order to facilitate a TEM image analysis of the three-dimensional clusters when projected onto a two-dimensional plane, we have studied the relationships between the cluster projected area and the number of monomers per aggregate and the relations between the three-dimensional and projected, two-dimensional lengths and the true cluster radius of gyration. Some important numerical results are summarized in Table 1. We find that DLCA aggregates retain a fractal morphol-

TABLE 1
Summary of Numerical Results for DLCA Aggregates Simulated on a Three-Dimensional Cubic Lattice

Fractal dimension and prefactor
$\delta = 1$ (monomer point contact)
$D = 1.80 \pm 0.03$, $k_0 = 1.30 \pm 0.07$
$\delta = 2$
$D = 2.01 \pm 0.03$, $k_0 = 3.0 \pm 0.08$
Length ratios
$R_g/R_3 = 0.61 \pm 0.03$
$R_g/R_2 = 0.69 \pm 0.03$
$R_2/R_3 = 0.89 \pm 0.03$

ogy, as defined by Eq. [1], as the degree of overlap between the monomers, i.e., primary particles, varies. Both the fractal dimension and the prefactor increase with the degree of overlap indicative of the densification of the cluster. The area versus number of monomers relationship is strongly affected by monomer overlap as depicted in Fig. 5. For point contact monomer clusters the length ratios determined from the simulations are best described by accounting for the anisotropic nature of the aggregates and use of a density correlation function that is cut off in a manner similar to that of a hard sphere.

Attempts to explain experimental discrepancies of the prefactor measured from real soot clusters, which otherwise are well described as DLCA aggregates with $D \simeq 1.8$, as due to cluster overlap were unsuccessful. In our simulation as the degree of overlap increases we find that both D and k_0 increase, while in some experiments the increase in k_0 was accompanied by the decrease in D. Hence the discrepancy among the experimental values of k_0 remains unsolved.

ACKNOWLEDGMENT

This work was supported by NSF Grant CTS 9408153.

REFERENCES

1. Forrest, S. R., and Witten, T. A., *J. Phys. A* **12,** L109 (1979).
2. Family, F., and Landau, D. P., (Eds.) "Kinetics of Aggregation and Gelation." North-Holland, Amsterdam, 1984.
3. Jullien, R., and Botet, R., "Aggregation and Fractal Aggregates." World Scientific, Singapore, 1987.
4. Samson, R. J., Mulholland, G. W., and Gentry, J. W., *Langmuir* **3,** 272 (1987).
5. Dobbins, R. A., and Megaridis, C. M., *Langmuir* **3,** 254 (1987).
6. Sorensen, C. M., and Feke, G. D., *Aerosol Sci. Tech.* **25,** 328 (1996).
7. Sorensen, C. M., Cai, J., and Lu, N., *Appl. Opt.* **31,** 6547 (1992).
8. Wu, M. K., and Friedlander, S. K., *J. Colloid Interface Sci.* **159,** 246 (1993).
9. Cai, J., Lu, N., and Sorensen, C. M., *J. Colloid Interface Sci.* **171,** 470 (1995).
10. Sorensen, C. M., and Roberts, G., *J. Colloid Interface Sci.* **186,** 447 (1997).
11. Puri, R., Richardson, T. F., Santoro, R. J., and Dobbins, R. A., *Combust. Flame* **92,** 320 (1993).
12. Koylu, U. O., Faeth, G. M., Farias, T. L., and Carvalho, M. G., *Combust. Flame* **100,** 621 (1995).
13. Koylu, U. O., and Faeth, G. M., *J. Heat Transfer* **116,** 152 (1994).
14. Koylu, U. O., and Faeth, G. M., *J. Heat Transfer* **116,** 971 (1994).
15. Koylu, U. O., Xing, Y., and Rosner, D. E., *Langmuir* **11,** 4848 (1995).
16. Sempere, R., Bourret, D., Woignier, T., Phalippou, J., and Jullien, R., *Phys. Rev. Lett.* **71,** 3307 (1993).
17. Weber, A. P., Baltensperge, U., Gaggeler, H. W., and Schmidt-Ott, A., *J. Aerosol Sci.* **27,** 915 (1996).
18. Medalia, A. I., and Heckman, F. A., *Carbon* **7,** 567 (1969).
19. Tence, M., Chevalier, J. P., and Jullien, R., *J. Phys. (Paris)* **47,** 1989 (1986).
20. Megaridis, C. M., and Dobbins, R. A., *Combust. Sci. Tech.* **71,** 95 (1990).
21. Meakin, P., *J. Colloid Interface Sci.* **102,** 491 (1984).
22. Rogak, S. N., Flagan, R. C., and Nguyen, H. V., *Aerosol Sci. Tech.* **18,** 25 (1993).
23. Cai, J., and Sorensen, C. M., *Phys. Rev. E* **50,** 3397 (1994).
24. Hurd, A. J., and Flower, W. L., *Colloid Interface Sci.* **122,** 178 (1988).
25. Botet, R., and Jullien, R., *J. Phys. A* **19,** L907 (1986).